Superior Toughness and Fast Self-Healing at Room Temperature Engineered by Transparent Elastomers

Seon-Mi Kim, Hyeonyeol Jeon, Sung-Ho Shin, Seul-A Park, Jonggeon Jegal, Sung Yeon Hwang, Dongyeop X. Oh,* and Jeyoung Park**

The most important properties of self-healing polymers are efficient recovery at room temperature and prolonged durability. However, these two characteristics are contradictory, making it difficult to optimize them simultaneously. Herein, a transparent and easily processable thermoplastic polyurethane (TPU) with the highest reported tensile strength and toughness (6.8 MPa and 26.9 MJ m^{-3}, respectively) is prepared. This TPU is superior to reported contemporary room-temperature self-healable materials and conveniently heals within 2 h through facile aromatic disulfide metathesis engineered by hard segment embedded aromatic disulfides. After the TPU film is cut in half and respliced, the mechanical properties recover to more than 75% of those of the virgin sample within 2 h. Hard segments with an asymmetric alicyclic structure are more effective than those with symmetric alicyclic, linear aliphatic, and aromatic structures. An asymmetric structure provides the optimal metathesis efficiency for the embedded aromatic disulfide while preserving the remarkable mechanical properties of TPU, as indicated by rheological and surface investigations. The demonstration of a scratch-detecting electrical sensor coated on a tough TPU film capable of auto-repair at room temperature suggests that this film has potential applications in the wearable electronics industry.

Self-healable polymers are promising smart materials because of their ability to autonomously repair physical damage, which extends their lifetime and reduces maintenance costs.[1] They can be used in a variety of fields such as surface protection coatings, healthcare materials, and sensors.[2] Research trends for self-healing polymers have shifted from extrinsic healing agents to intrinsic, from high to low healing temperatures, from mellow gels to robust elastomers, and from translucent films to transparent films in order to improve the user experience. However, the self-healing efficiency and robustness of the material are contradictory properties and are difficult to optimize simultaneously.[2e,3]

S.-M. Kim, Dr. H. Jeon, S.-H. Shin, S.-A Park, Dr. J. Jegal, Prof. S. Y. Hwang, Prof. D. X. Oh, Prof. J. Park
Research Center for Bio-Based Chemistry
Korea Research Institute of Chemical Technology (KRICT)
Ulsan 44429, Republic of Korea
E-mail: crew75@krict.re.kr; dongyeop@krict.re.kr; jypark@krict.re.kr
Prof. S. Y. Hwang, Prof. D. X. Oh, Prof. J. Park
Advanced Materials and Chemical Engineering
University of Science and Technology (UST)
Daejeon 34113, Republic of Korea

The ORCID identification number(s) for the author(s) of this article can be found under https://doi.org/10.1002/adma.201705145.

DOI: 10.1002/adma.201705145

To realize a robust, transparent, and easily processable polymer that is intrinsically self-healable at room temperature, the following three material design criteria were established: (1) a readily processable and physically tunable base material, (2) a dynamic covalent bond that is operable at room temperature, and (3) optimal self-healing efficiency and mechanical properties.

Thermoplastic polyurethane (TPU) is a thermoprocessable elastomer that is widely used as a protective film in the automotive and electronic industries. TPU was selected as the base material to satisfy the first criterion because its chemical structure can be fine-tuned to generate the desired transparency and mechanical properties.[4] Urethane structures containing polytetramethylene ether glycol (PTMEG) have been utilized to prepare shape memory effect-assisted self-healing materials.[5]

To satisfy the second criterion, an aromatic disulfide bond was selected as the chemical operator.[6] Intrinsic self-healing is chemically driven by noncovalent bonds such as hydrogen bonds,[3c–e,5c,7] metal–ligand,[8] host–guest interactions,[2e,9] or reversible (dynamic) covalent bonds[10] such as Diels–Alder,[11] radical recombination,[12] urea chemistry,[13] olefin metathesis,[14] polysiloxanes,[15] boronic esters,[16] acylhydrazones,[17] and other reactions.[18] Among these, disulfide metathesis has attracted significant attention since it can be activated at moderate temperatures (60–90 °C) and without external stimuli.[5d,19] In particular, an aromatic disulfide-based poly(urea-urethane) shows efficient room-temperature self-healing because aromatic disulfides undergo more efficient metathesis than aliphatic disulfides.[6e,f,20]

The third criterion was addressed by optimizing the mechanical properties and self-healing efficiency of TPU through the design of a hard segment of the polymer containing the chemical operator, i.e., an aromatic disulfide moiety. Generally, TPUs with tightly packed hard segments have better mechanical properties but lower self-healing efficiency because the restricted chain mobility hinders disulfide metathesis.[5d,21] Loosely packed hard segments produce the opposite effect. Room-temperature self-healable cross-linked poly(urea-urethane) has an undesirable ultimate tensile strength (UTS) of ≈0.8 MPa with a toughness of ≈13 MJ m^{-3}.[6e] Other disulfide-containing TPUs have UTS values greater than 10 MPa, but they must be heated above 80 °C to initiate self-healing.[5d]

 © 2017 WILEY-VCH Verlag GmbH & Co. KGaA, Weinheim

Based on these three criteria, we designed a processable and transparent TPU with the highest concurrent UTS and toughness values (6.8 MPa and 26.9 MJ m^{-3}, respectively) reported to date for room-temperature self-healing polymers[2e,6e,g,7a,c,8b–d,14,16a,17b,18c,e,19e,f] and efficient self-healing at room temperature within 2 h. In our TPU system, crystalline PTMEG was used as a soft segment and bis(4-hydroxyphenyl) disulfide (**SS**) was used as the aromatic disulfide component embedded in the hard segments. Among the various hard segment candidates, isophorone diisocyanate (**IP**) was the most effective in terms of transparency, self-healing efficiency, and mechanical properties of the resultant TPU. The asymmetric alicyclic structure of **IP** provides sufficient chain mobility to activate disulfide metathesis while retaining the remarkable mechanical properties. As a proof-of-concept, we demonstrated the application of a scratch-detecting and auto-repairing electrical sensor coated on the TPU film.

The synthetic routes to the TPUs are shown in **Figure 1**a. We propose that the self-healing efficiency and mechanical properties of TPU are both dependent on the packing density of the hard segment domains. To confirm this assumption, the following four diisocyanates with different molecular structures were introduced into the TPUs as hard segment units: **IP** (asymmetric alicyclic structure); 4,4′-methylenebis(cyclohexyl isocyanate) (**HM**; symmetric alicyclic structure); 4,4′-methylenebis(phenyl isocyanate) (**M**; aromatic structure); and hexamethylene diisocyanate (**H**; linear aliphatic structure).

To synthesize a bis-isocyanate-terminated preoligomer, PTMEG (as a soft segment diol) was reacted with two equivalents of each diisocyanate monomer in *N,N′*-dimethylacetamide (DMAc) in the presence of dibutyltin dilaurate as a catalyst. Then, **SS** (an aromatic disulfide) or ethylene glycol (**EG**, a control) was added to the solution as a chain extender to complete the TPU synthesis. Detailed polymerization procedures,

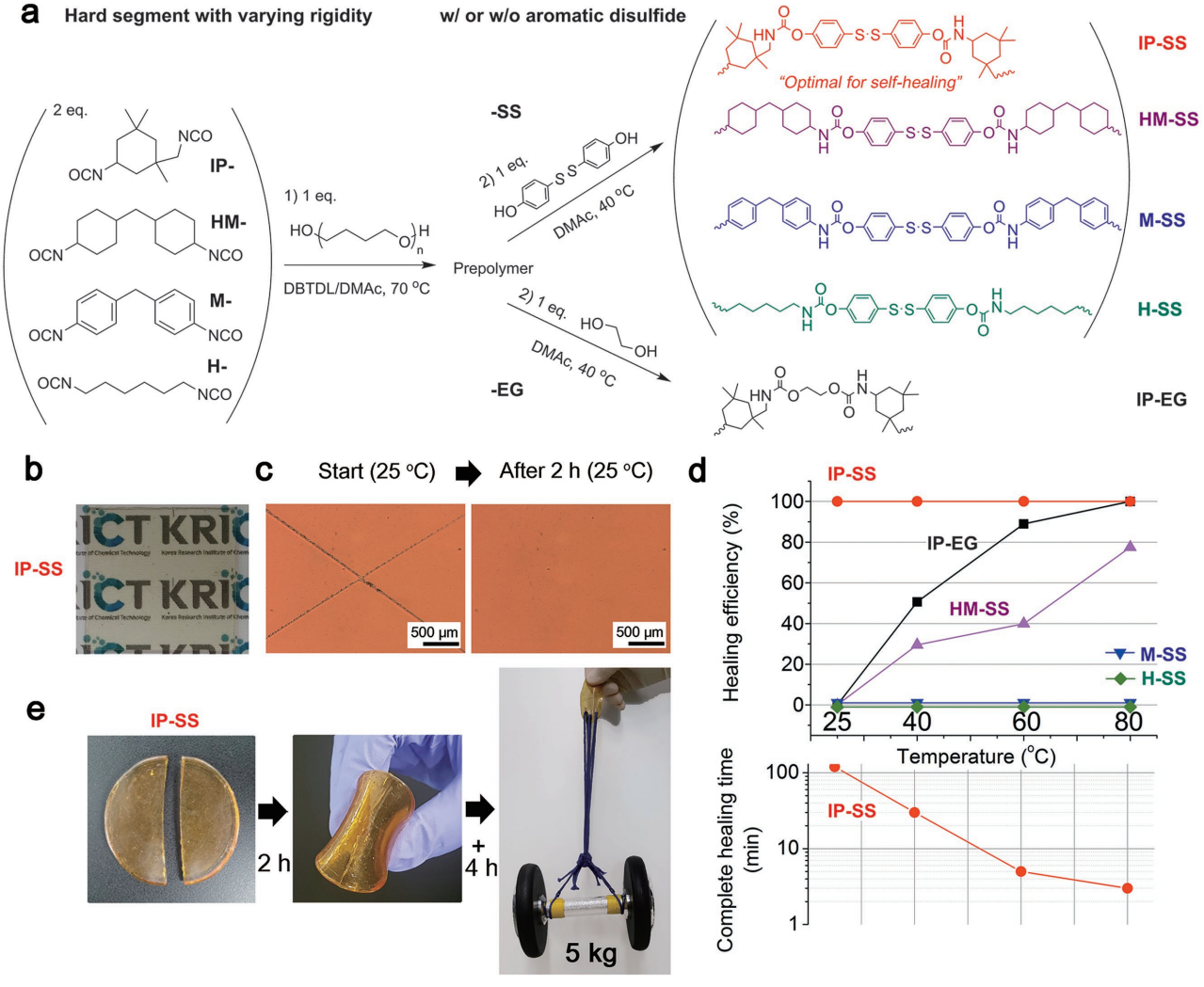


Figure 1. a) Synthetic routes to TPUs with four different diisocyanates (i.e., **IP**, **HM**, **M**, and **H**) and two chain extenders (i.e., **SS** and **EG**). The TPUs are designated as X–Y, where X and Y denote the abbreviation of the diisocyanate monomer and chain extender, respectively. b) Photograph of the TPU film (25 mm × 25 mm × 0.3 mm) of **IP–SS**. c) Optical microscopy images of the X-shaped scratch on the TPU film of **IP–SS** before and after healing for 2 h at 25 °C. d) Top: healing efficiencies after 2 h at 25 °C and 1 h at 40, 60, and 80 °C. Bottom: time required for full scratch recovery of **IP–SS** with respect to temperature. e) **IP–SS** film cut in half, respliced, and healed for 2 h (+4 h) at 25 °C, followed by a 5 kg dumbbell lifting test.

© 2017 WILEY-VCH Verlag GmbH & Co. KGaA, Weinheim

polymerization results, and ^{1}H NMR spectroscopic data are included in the Experimental Section, Table S1, and Figure S1 (Supporting Information).

All TPUs showed moderate solution viscosities and comparable molecular weights, as measured by gel permeation chromatography (Figure S2, Supporting Information). This indicates that all the TPUs are solution-processable and that the **SS** group did not cause gelation during polymerization. All **SS**-containing TPU solutions of DMAc were pale yellow due to the characteristics of the disulfides, while the **IP–EG** solution was colorless (Figure S3, Supporting Information).[6e,20] The **H–SS** solution was translucent because the aliphatic chain of **H** induced crystallization,[5d] while the other TPU solutions of DMAc were transparent.

Films were prepared from each of the TPUs via solvent casting (Figure 1b and Figure S4 (Supporting Information)). All the TPU films had similar appearances as their respective original DMAc solutions in terms of color and transparency. Transmission spectra of the TPU films with a thickness of 150 µm suggested that the transparency increases in the order **H–SS** < **M–SS** < **HM–SS** < **IP–SS** < **IP–EG**, and that the transmittance of **IP–SS** at 550 nm was over 94.9%, with the film thickness being up to 470 µm (Figures S5 and S6, Supporting Information). In contrast to the other films, the **H–SS** film was translucent and had a heterogeneous surface with aggregates of 10^1–10^2 µm. The **IP**-, **HM**-, and **M**-containing TPUs were amorphous, while the **H**-containing TPU was semicrystalline due to its linear aliphatic structure.[5d] Thus, a linear aliphatic hard segment, (**H**), does not generate a transparent TPU.

Attenuated total reflectance Fourier transform infrared spectra of all the TPU films featured negligible peaks at 2264 and 1743 cm^{-1}, which correspond to the N=C=O stretching band and C=O stretching band of DMAc, respectively. This suggests that the diisocyanate monomers were fully converted to urethane bonds and DMAc was completely removed during the solvent casting, which was confirmed to distinguish solvent-mediated chain mobility from self-healing (Figure S7, Supporting Information).

The self-healing properties were first evaluated by a scratch recovery test.[22] TPU films with 30–70 µm wide scratches were placed on a heating stage at the desired temperature and the scratch width was monitored using optical microscopy. The microscopic images are shown in Figure 1c and Figures S4 and S8 (Supporting Information). The healing efficiency (%) is defined as 100 × [1 − (final width)/(initial width)] and reported as the average value of five experiments.

The **IP–SS** film was the only one to achieve full scratch recovery, i.e., a healing efficiency of 100% within 120 min at 25 °C, while the other TPUs, including **IP–EG**, showed no scratch recovery, i.e., a healing efficiency of 0% at 25 °C (Figure 1d and Movie S1 (Supporting Information)). This suggests that the **SS** moiety was necessary for the self-healing of the **IP–SS** film. Because of the increasing chain mobility at higher temperatures, the time required for full scratch recovery of the **IP–SS** film decreased with temperature requiring only 30, 5, and 3 min at 40, 60, and 80 °C, respectively.[12c]

To visualize the superior self-healing properties of **IP–SS**, a circular film sample with a diameter of 46.0 mm and thickness of 2.0 mm was cut in half and respliced at room temperature. After 2 h, the self-healed **IP–SS** film withstood manual drawing. After a further 4 h, it was able to lift a weight of 5 kg without tearing (Figure 1e and Movie S2 (Supporting Information)).

The healing efficiencies of the TPUs increased in the following order: **IP–SS** > **IP–EG** > **HM–SS** > **M–SS** ≈ **H–SS**. From these results, two phenomena are evident that are worth discussing. First, **M–SS** and **H–SS** showed no self-healing ability, even at 80 °C, though they contain similar molar ratios of **SS** as **IP–SS**. Unlike **IP–SS**, **M–SS** and **H–SS** have tightly packed hard segment domains because the **M** and **H** moieties form additional π–π stacking and crystalline structures, respectively. Therefore, the **SS** moieties embedded in the **M** and **H** hard segments could not undergo disulfide metathesis because of the restricted chain segmental motion. This issue will be further discussed in the rheology section.

Second, **IP–EG** has the second highest healing efficiency of the TPUs at temperatures greater than 40 °C, even though it does not contain the **SS** moiety. Among the TPUs, **IP–EG** has the highest degree of chain segmental motion because of the combination of an aliphatic chain extender, **EG**, and an asymmetric alicyclic diisocyanate, **IP**. Thus, the **EG** matrix likely flows to fill the scratch valley at elevated temperatures.

To evaluate the mechanical properties and self-healing efficiencies of the TPU samples, tensile tests were conducted using a universal tensile machine. Conventional tensile tests with a typical drawing rate of 100 mm min^{-1} were conducted, and the UTS, elongation at break, and toughness of the TPUs were measured and are summarized in Figure S9 and Table S2 (Supporting Information). The UTS values of the TPU films increased in the following order: **M–SS** > **H–SS** > **HM–SS** > **IP–SS** > **IP–EG**. This suggests that the UTS is directly dependent on the packing density of the hard segments. **M–SS** and **H–SS** achieved UTS values of 30.4 and 9.5 MPa, respectively, due to their rigid aromatic and crystalline hard segment domains, respectively. It should be emphasized that the UTS and these toughness values of **IP–SS** reached 6.8 MPa and 26.9 MJ m^{-3}, respectively, and these values are estimated to be the highest reported to date for room-temperature self-healing polymers (**Figure 2**a,b and **Table 1** and Movie S3 (Supporting Information)). The highly robust TPU of **IP–SS** is the first introduced material featuring a crystalline PTMEG of soft segment-assisted toughness and shape memory effect for facile self-healing. The asymmetric alicyclic structure of **IP** in the hard segment enabled chain mobility for effective disulfide metathesis and increased transparency. In addition, there were no cross-linkers disrupting the phase separation for high tenacity and elongation.

Long-term air stability of the disulfides from oxidation-mediated cleavage of the polymer chains was checked by time-aging mechanical testing. The results of the tensile experiments of **IP–SS** films exposed to ambient laboratory conditions were consistent over a one month period (Figure S10, Supporting Information). Self-healing properties were also maintained, relieving fundamental concerns about practical use.

To investigate the self-healing efficiency, tensile experiments on cut and respliced TPU samples were performed as follows: TPU films were cut in half and both pieces were then realigned with an overlap of 2 mm × 6 mm at 25 °C for varying time periods. Overall, **IP–SS** has the best self-healing efficiency

© 2017 WILEY-VCH Verlag GmbH & Co. KGaA, Weinheim

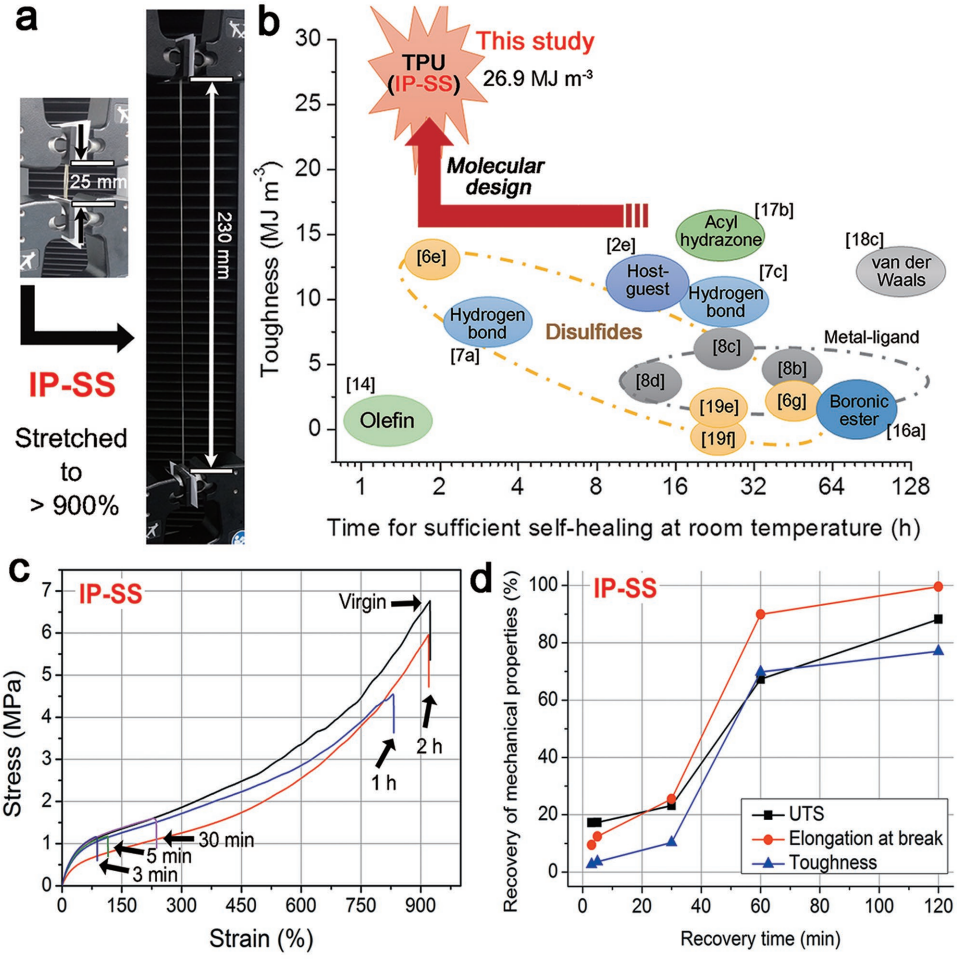


Figure 2. a) Photographs of an **IP–SS** film before and after stretching. b) Ashby plot of "toughness" versus "time for sufficient self-healing at room temperature" of **IP–SS** and other room-temperature self-healable polymers reported in literature. c) The tensile stress–strain curves and d) the recovery (%) of UTS, elongation at break, and toughness of virgin **IP–SS** and cut and respliced **IP–SS** with different healing times.

(Figure 2c,d), and the recovery of UTS, elongation, and toughness increased over time. For **IP–SS**, a healing time of 2 h resulted in 88.2%, 99.6%, and 76.6% recovery of the UTS, elongation at break, and toughness values of the virgin **IP–SS**, respectively. In accordance with the scratch recovery tests, the respliced samples of **M–SS** and **H–SS** presented mechanical recoveries of <5% at 25 °C. In contrast, the respliced samples of **IP–EG** and **HM–SS** showed moderate mechanical recoveries at 25 °C (Figure S11 and Table S2, Supporting Information). These results do not match with the results of the scratch recovery tests, which showed no healing at 25 °C and indicate that **IP–EG** and **HM–SS** have pressure-sensitive self-healing properties. Also, it suggests that the mechanical recovery of the respliced TPUs is not caused by disulfide metathesis-mediated cohesion but rather by noncovalent bond-mediated adhesion.

To separate the roles of noncovalent bond-mediated adhesion from disulfide methathesis (main self-healing factor), the adhesion energies of the TPUs on glass were analyzed using a shear adhesion strength test.[2c,d] A TPU film sample with dimensions of 10 mm × 10 mm was placed between two slide glasses and pressed under a 50 g plumb for 2 h before the shear adhesion strength measurement. Among the TPUs, **IP–EG** showed the highest shear adhesion strength of 0.33 MPa, which is 1.8, 3.1, and 6.2 times higher than the values for **IP–SS**, **HM–SS**, and **M–SS**, respectively (Figure S12, Supporting Information). This is presumably because of the high molecular mobility of **IP–EG** enabling high molecular penetration into the surface pores and high molecular diffusion on the surface.[23] The poor adhesion strengths of **IP–SS** and **HM–SS** indicate that the disulfide metathesis-mediated cohesion dominates the mechanical recovery of the respliced **IP–SS** and **HM–SS**, whereas noncovalent bond-mediated adhesion was the main contributor to the pressure-sensitive resplicing of **IP–EG**.

The crack-healing mechanism of the polymers can be divided into the following five steps:[24] (1) surface rearrangement, (2) surface approach, (3) wetting, (4) diffusion, and (5) randomization. Wetting and diffusion are functions of chain mobility, which can be characterized by rheometry and dynamic mechanical analysis (DMA). In contrast, randomization is driven by disulfide metathesis.

To further understand the self-healing behavior from a rheological perspective, frequency sweep and step-strain experiments were conducted on the TPUs at 25 and 60 °C.[25] The TPUs appeared to be elastic solids at 25 °C, with G' displaying

© 2017 WILEY-VCH Verlag GmbH & Co. KGaA, Weinheim

Table 1. Estimated UTS, elongation at break, toughness, and recovery tests of various self-healing polymers at room temperature.

Self-healing motif	Virgin			Time for self-healing, efficiency over 80% [h]	Repaired			Ref.
	Ultimate tensile strength [MPa]	Elongation at break [%]	Toughness [MJ m^{-3}]		Ultimate tensile strength [MPa]	Elongation at break [%]	Toughness [MJ m^{-3}]	
Disulfides	6.76	923	26.9	2	5.96	920	20.6	This study
	0.81	3100	13	2	0.65	2625	8.5	[6e]
	4.3	128	3.1	48	3.7	113	2.6	[6g]
	0.392	202	0.5	24[a)]	0.382	175	0.4	[19e]
	0.23	105	0.13	24	0.21	100	0.12	[19f]
Acylhydrazone	0.297	11 700	14.1	24	0.247	10 650	10.7	[17b]
van der Waals	4.4	560	12	120	4.4	500	11	[18c]
Host–guest	0.5	>4500	>11	12	0.5	>4500	>11	[2e]
Hydrogen bonding	1.9	780	10	24	1.7	710	8	[7c]
	3.4	600	8	3	2.9	520	6	[7a]
Catechol	3.5	310	6.8	24	4.2	190	5.3	[8c]
Diselenide	2.1	700	6.6	24	1.6	620	4.5	[18e]
Metal–ligand	0.23	1850	3.8	48	0.22	1700	3.4	[8b]
	0.30	1400	3.4	12	0.32	1500	3.8	[8d]
Boronic ester	4.4	58	1.4	72	4	53	1.2	[16a]
Olefin	0.4	100	0.25	1[b)]	0.4	100	0.25	[14]

[a)]Self-healed under visible light irradiation; [b)]Self-healed under a pressure of 20 kPa.

a higher modulus than G'' in the frequency sweep graph (Figure S13, Supporting Information). The occurrence of a crack or scratch generates mechanical or thermodynamic stress because it increases the interfacial area. The relaxation time (λ) is the time required for a viscous material to recover from mechanical or thermodynamic stress. Thus, λ is a good indicator to quantify self-healing efficiency.[26] In addition, λ is a function of chain mobility with respect to analogous polymers.[27]

The relation between λ and frequency can be calculated from the frequency sweep graph (**Figure 3**a,b).[27,28] **IP–SS** showed the lowest λ among the TPUs over the entire frequency range at both temperatures, which correlates with **IP–SS** showing the highest self-healing efficiencies in both the scratch and resplicing tests. This suggests that the kinetics of disulfide exchange in **IP–SS** are faster than those of the other **SS**-containing TPUs due to the loosely packed hard segments. Since **IP–SS** has a lower λ than **IP–EG**, it is likely that, along with the high chain mobility, disulfide metathesis is necessary for room-temperature self-healing in this system. As the temperature increased from 25 to 60 °C, the λ of **IP–EG** decreased to as low as that of **IP–SS** over the entire frequency range. These data correlate well with the result for the scratch recovery of **IP–EG** at 60 °C. For the **SS**-containing TPUs, λ generally increased in the order of **IP** < **HM** < **M** ≈ **H**, which suggests that the packing density of the hard segments increases in the order of **IP** < **HM** < **M** ≈ **H**.

In the step-strain experiments at 25 and 60 °C (Figure 3c,d),[26] **IP–SS** exhibits notably lower stress relaxation toward a zero stress state depending on time after 5% shear strain than the other TPUs. The trends of the stress relaxation data according to types of samples and temperatures are analogous to the λ data.

To further elucidate the self-healing properties from the perspective of surface chemistry, narrow X-ray photoelectron spectroscopy (XPS) scans of **IP–SS**, **HM–SS**, and **M–SS** were conducted (Figure 3e–h). The general sampling depth of XPS is ≈1–6 nm.[29] Thus, the XPS can clarify the disulfide metathesis behavior between cracked surfaces. Self-healable **IP–SS** showed a higher intensity of sulfur (S) 2p and nitrogen (N) 1s peaks than nonhealable **HM–SS** and **M–SS**; this indicates that the disulfide and adjacent urethane moieties are possibly more prevalent on the surface of **IP–SS** than on the surfaces of **HM–SS** and **M–SS**. The **SS** moieties of **IP–SS** could more easily migrate to the surface because of the loosely packed hard segments. In contrast, **HM–SS** and **M–SS**, which are nonhealable at room temperature, showed higher intensities of oxygen (O) 1s peaks, which is likely because the PTMEG moieties are more prevalent on the surface. The more flexible PTMEG moieties could more readily migrate toward the surface than the **SS** moieties embedded in the tightly packed **M**- and **HM**-based domains.[30] Overall, the XPS data suggest that the higher surface exposure of the **SS** groups of **IP–SS** than those of **HM–SS** and **M–SS** promotes enhanced disulfide metathesis at the crack interface. Meanwhile, it was difficult to obtain reproducible XPS data for **H–SS** because the maximum beam size (50 μm) of XPS is smaller than the heterogeneous aggregate (Figure S4, Supporting Information) of **H–SS** due to its high crystallinity.

Loss tangent delta (tanδ) over the temperature range of –80 to 60 °C of TPUs was obtained using DMA (Figure S14, Supporting Information). **M–SS** and **H–SS** showed typical tanδ patterns with a single peak assigned to the glass transition temperature (T_g). However, in the tanδ patterns of **IP–SS**, **IP–EG**, and **HM–SS**, there was an ambiguous peak, and tanδ gradually increased between 25 and 60 °C. In the matrices of

© 2017 WILEY-VCH Verlag GmbH & Co. KGaA, Weinheim

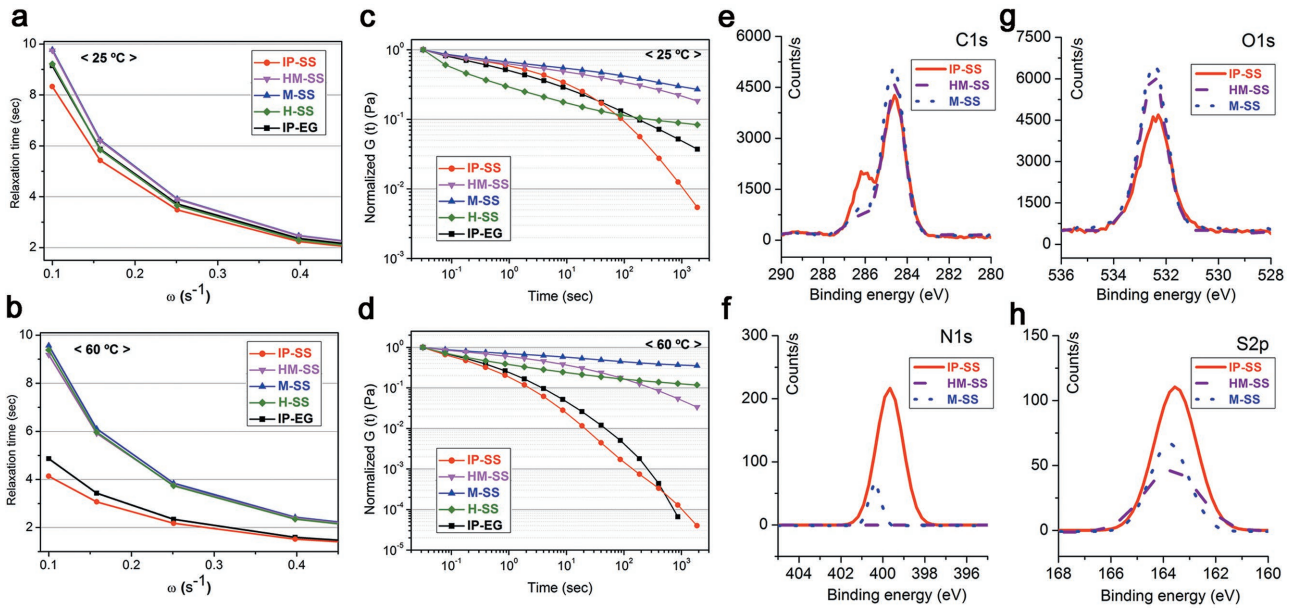


Figure 3. Plots of relaxation time (λ) versus frequency at a) 25 °C and b) 60 °C obtained from a frequency sweep test. Stress relaxation versus time plots at c) 25 °C and d) 60 °C, as obtained from a step-strain experiment. XPS spectra of e) C 1s, f) N 1s, g) O 1s, and h) S 2p region of **IP–SS** (red solid line), **HM–SS** (purple dashed line), and **M–SS** (blue dotted line).

M–SS and **H–SS**, the **M** and **H** moieties are tightly packed, and their domains localized away from soft segments, i.e., PTMEG. Thus, the localized PTMEG resulted in the clear and lower T_g peaks for **M–SS** and **H–SS**. In the matrices of **IP–SS**, **IP–EG**, and **HM–SS**, the soft segments are not well localized because of the poorly packed hard segments, thereby resulting in unclear T_g peaks. The low packing density of the hard segments resulted in larger energy dissipation upon stress induction.

The phenomenological and analytical data revealed that the self-healing efficiencies of the TPUs increased in the following order: **IP–SS** > **IP–EG** ≥ **HM–SS** > **H–SS** ≈ **M–SS**. **IP–SS** almost fully recovered from the surface scratch and mechanical break within 2 h at 25 °C. **HM–SS** showed no scratch recovery but presented moderate resplicing properties under pressure at room temperature. However, **H–SS** and **M–SS** did not self-heal at room temperature. It is possible that the alicyclic structures of **IP** and **HM** resulted in looser packing than that of the aromatic **M** and crystalline **H**, thereby promoting disulfide metathesis (**Figure 4**a). Asymmetric and kinked **IP** had a more loosely packed structure than **HM**, as revealed by the rheology and dynamic mechanical studies.

The incorporation of loosely packed **IP** moieties was achieved while retaining the remarkable mechanical properties of TPU. This can be understood by discussing a similar example, 1,4-cyclohexanedimethanol (CHDM). CHDM is a unique alicyclic monomer with ring flip-mediated increased mobility of the polymer chain.[31] The incorporation of CHDM into a polyester or polycarbonate can increase the degree of polymerization

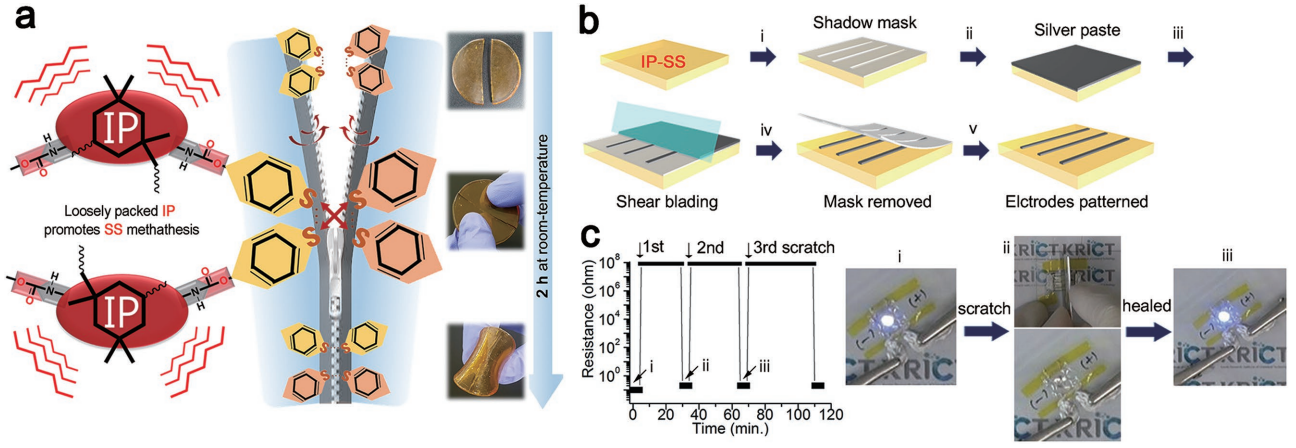


Figure 4. Illustration of a) the optimal self-healing process of **IP–SS**, and b) the process of preparing the scratch-detecting electrical sensor by the stencil printing method ((i): covering a shadow mask of width of 500 µm and thickness of 50 µm on the **IP–SS** film, (ii): applying a silver paste, (iii): shear blading with a slide glass, (iv): removing the shadow mask, (v): electrodes patterned and interconnected with an LED). c) Resistance changes of the sensor for three scratches at the same location ((i): light-on at pristine stage, (ii): light-off after scratch, (iii): light-on after electrical healing at 25 °C).

© 2017 WILEY-VCH Verlag GmbH & Co. KGaA, Weinheim

because the moiety reduces the reaction viscosity without affecting the mechanical properties of the polymer product. In a similar way, the unique alicyclic structure of **IP** improved both the self-healing efficiency and mechanical durability.

Because of its unique durability and elasticity, the **IP–SS** has promising application in wearable sensors that can repair after routine scratches. Exemplary application of these self-healing materials was demonstrated by preparing a scratch-detecting and auto-repairing electrical sensor. A stencil printing method was applied to pattern microsized silver electrodes on the **IP–SS** film (Figure 4b). After the first scratch caused an increase in the resistance over mega ohms (light-off), the pristine resistance and light-on could be recovered within 25 min at 25 °C (Figure 4c and Figure S15 and Movie S4 (Supporting Information)). Repeated scratching at the same location was performed to test the intrinsic healing of the material. The total electrical rehealing times were 30 min for the second scratch and 40 min for the third scratch. Electrical healing occurred only with the base material (**IP–SS**) and without external stimuli such as artificial reunion of the cut surfaces under pressure, as reported previously.[2b,8f,g,18g]

In summary, we developed a transparent, easily processable, quickly self-healing TPU at room temperature (**IP–SS**) with robustness, stretchability, and durability surpassing those of current room-temperature self-healable materials. The toughness value of 26.9 MJ m^{-3} was twice the best value for a previously reported material. The key is the incorporation of **IP**—which has a unique alicyclic structure—as the hard segment embedding aromatic disulfide. The **IP**-based hard segment domains had adequate packing density to achieve efficient self-healing and to retain the remarkable mechanical properties of TPU. Based on the demonstration of a scratch-detecting and auto-repairing electrical sensor coated on **IP–SS**, we suggest that this robust self-healing TPU is a promising base material in various industries.

Experimental Section

Experimental details are given in the Supporting Information.

Supporting Information

Supporting Information is available from the Wiley Online Library or from the author.

Acknowledgements

This research was supported by the Ministry of Trade, Industry & Energy (MOTIE), the Korea Institute for Advancement of Technology (KIAT), and the Ulsan Institute for Regional Program Evaluation (IRPE) through the Encouragement Program for The Industries of Economic Cooperation Region (R0004879).

Conflict of Interest

The authors declare no conflict of interest.

Keywords

aromatic disulfide, room-temperature self-healing, thermoplastic polyurethane, toughness

Received: September 8, 2017
Revised: September 27, 2017
Published online: November 13, 2017

[1] a) D. Y. Wu, S. Meure, D. Solomon, *Prog. Polym. Sci.* **2008**, *33*, 479; b) J. A. Syrett, C. R. Becer, D. M. Haddleton, *Polym. Chem.* **2010**, *1*, 978; c) N. K. Guimard, K. K. Oehlenschlaeger, J. Zhou, S. Hilf, F. G. Schmidt, C. Barner-Kowollik, *Macromol. Chem. Phys.* **2012**, *213*, 131; d) F. Herbst, D. Döhler, P. Michael, W. H. Binder, *Macromol. Rapid Commun.* **2013**, *34*, 203; e) S. Billiet, X. K. D. Hillewaere, R. F. A. Teixeira, F. E. Du Prez, *Macromol. Rapid Commun.* **2013**, *34*, 290; f) Y. Yang, M. W. Urban, *Chem. Soc. Rev.* **2013**, *42*, 7446; g) P. Michael, D. Döhler, W. H. Binder, *Polymer* **2015**, *69*, 216.

[2] a) S. H. Cho, S. R. White, P. V. Braun, *Adv. Mater.* **2009**, *21*, 645; b) S. J. Benight, C. Wang, J. B. Tok, Z. Bao, *Prog. Polym. Sci.* **2013**, *38*, 1961; c) B. J. Kim, D. X. Oh, S. Kim, J. H. Seo, D. S. Hwang, A. Masic, D. K. Han, H. J. Cha, *Biomacromolecules* **2014**, *15*, 1579; d) D. X. Oh, S. Kim, D. Lee, D. S. Hwang, *Acta Biomater.* **2015**, *20*, 104; e) J. Liu, C. S. Y. Tan, Z. Yu, N. Li, C. Abell, O. A. Scherman, *Adv. Mater.* **2017**, *29*, 1605325; f) J. Cao, C. Lu, J. Zhuang, M. Liu, X. Zhang, Y. Yu, Q. Tao, *Angew. Chem., Int. Ed.* **2017**, *56*, 8795.

[3] a) R. J. Wojtecki, M. A. Meador, S. J. Rowan, *Nat. Mater.* **2011**, *10*, 14; b) J. A. Neal, D. Mozhdehi, Z. Guan, *J. Am. Chem. Soc.* **2015**, *137*, 4846; c) H. J. Zhang, T. L. Sun, A. K. Zhang, Y. Ikura, T. Nakajima, T. Nonoyama, T. Kurokawa, O. Ito, H. Ishitobi, J. P. Gong, *Adv. Mater.* **2016**, *28*, 4884; d) J. Wu, L.-H. Cai, D. A. Weitz, *Adv. Mater.* **2017**, *29*, 1702616; e) S. Yoshida, H. Ejima, N. Yoshie, *Adv. Funct. Mater.* **2017**, *27*, 1701670.

[4] H. W. Engels, H. G. Pirkl, R. Albers, R. W. Albach, J. Krause, A. Hoffmann, H. Casselmann, J. Dormish, *Angew. Chem., Int. Ed.* **2013**, *52*, 9422.

[5] a) G. Rivero, L.-T. T. Nguyen, X. K. D. Hillewaere, F. E. Du Prez, *Macromolecules* **2014**, *47*, 2010; b) A. Feula, A. Pethybridge, I. Giannakopoulos, X. Tang, A. Chippindale, C. R. Siviour, C. P. Buckley, I. W. Hamley, W. Hayes, *Macromolecules* **2015**, *48*, 6132; c) M. Wei, M. Zhan, D. Yu, H. Xie, M. He, K. Yang, Y. Wang, *ACS Appl. Mater. Interfaces* **2015**, *7*, 2585; d) Y. Xu, D. Chen, *Macromol. Chem. Phys.* **2016**, *217*, 1191.

[6] a) R. J. Sarma, S. Otto, J. R. Nitschke, *Chem. - Eur. J.* **2007**, *13*, 9542; b) A. M. Belenguer, T. Friscic, G. M. Day, J. K. M. Sanders, *Chem. Sci.* **2011**, *2*, 696; c) J. M. Matxain, J. M. Asua, F. Ruiperez, *Phys. Chem. Chem. Phys.* **2016**, *18*, 1758; d) S. Nevejans, N. Ballard, J. I. Miranda, B. Reck, J. M. Asua, *Phys. Chem. Chem. Phys.* **2016**, *18*, 27577; e) A. Rekondo, R. Martin, A. R. de Luzuriaga, G. Cabañero, H. J. Grande, I. Odriozola, *Mater. Horiz.* **2014**, *1*, 237; f) R. Martin, A. Rekondo, A. R. de Luzuriaga, G. Cabañero, H. J. Grande, I. Odriozola, *J. Mater. Chem. A* **2014**, *2*, 5710; g) R. H. Aguirresarobe, L. Martin, M. J. Fernandez-Berridi, L. Irusta, *eXPRESS Polym. Lett.* **2017**, *11*, 266.

[7] a) P. Cordier, F. Tournilhac, C. Soulie-Ziakovic, L. Leibler, *Nature* **2008**, *451*, 977; b) J. Hentschel, A. M. Kushner, J. Ziller, Z. Guan, *Angew. Chem., Int. Ed.* **2012**, *124*, 10713; c) Y. Chen, A. M. Kushner, G. A. Williams, Z. Guan, *Nat. Chem.* **2012**, *4*, 467; d) Y. Chen, Z. Guan, *Chem. Commun.* **2014**, *50*, 10868; e) G. Gao, G. Du, Y. Sun, J. Fu, *ACS Appl. Mater. Interfaces* **2015**, *7*, 5029; f) S. Chen, X. Bi, L. Sun, J. Gao, P. Huang, X. Fan, Z. You, Y. Wang, *ACS Appl. Mater. Interfaces* **2016**, *8*, 20591; g) S. Chen, W. H. Binder, *Acc. Chem. Res.* **2016**, *49*, 1409; h) I. Jeon, J. Cui, W. R. K. Illeperuma, J. Aizenberg, J. J. Vlassak, *Adv. Mater.* **2016**, *28*, 4678.

 © 2017 WILEY-VCH Verlag GmbH & Co. KGaA, Weinheim

[8] a) M. Burnworth, L. Tang, J. R. Kumpfer, A. J. Duncan, F. L. Beyer, G. L. Fiore, S. J. Rowan, C. Weder, *Nature* **2011**, *472*, 334; b) C.-H. Li, C. Wang, C. Keplinger, J.-L. Zuo, L. Jin, Y. Sun, P. Zheng, Y. Cao, F. Lissel, C. Linder, X.-Z. You, Z. Bao, *Nat. Chem.* **2016**, *8*, 618; c) J. Li, H. Ejima, N. Yoshie, *ACS Appl. Mater. Interfaces* **2016**, *8*, 19047; d) J.-F. Mei, X.-Y. Jia, J.-C. Lai, Y. Sun, C.-H. Li, J.-H. Wu, Y. Cao, X.-Z. You, Z. Bao, *Macromol. Rapid Commun.* **2016**, *37*, 1667; e) M. Haring, D. D. Diaz, *Chem. Commun.* **2016**, *52*, 13068; f) Y. Shi, M. Wang, C. Ma, Y. Wang, X. Li, G. Yu, *Nano Lett.* **2015**, *15*, 6276; g) F. Zhao, Y. Shi, L. Pan, G. Yu, *Acc. Chem. Res.* **2017**, *50*, 1734.

[9] a) P. Wei, X. Yan, F. Huang, *Chem. Soc. Rev.* **2015**, *44*, 815; b) M. Nakahata, Y. Takashima, H. Yamaguchi, A. Harada, *Nat. Commun.* **2011**, *2*, 511; c) M. Zhang, D. Xu, X. Yan, J. Chen, S. Dong, B. Zheng, F. Huang, *Angew. Chem., Int. Ed.* **2012**, *124*, 7117.

[10] a) T. Maeda, H. Otsuka, A. Takahara, *Prog. Polym. Sci.* **2009**, *34*, 581; b) Y. Jin, C. Yu, R. J. Denman, W. Zhang, *Chem. Soc. Rev.* **2013**, *42*, 6634; c) Z. Wei, J. H. Yang, J. Zhou, F. Xu, M. Zrinyi, P. H. Dussault, Y. Osada, Y. M. Chen, *Chem. Soc. Rev.* **2014**, *43*, 8114; d) N. Roy, B. Bruchmann, J.-M. Lehn, *Chem. Soc. Rev.* **2015**, *44*, 3786; e) F. García, M. M. J. Smulders, *J. Polym. Sci., Part A: Polym. Chem.* **2016**, *54*, 3551; f) W. Zou, J. Dong, Y. Luo, Q. Zhao, T. Xie, *Adv. Mater.* **2017**, *29*, 1606100.

[11] a) Y.-L. Liu, T.-W. Chuo, *Polym. Chem.* **2013**, *4*, 2194; b) X. Chen, M. A. Dam, K. Ono, A. Mal, H. Shen, S. R. Nutt, K. Sheran, F. Wudl, *Science* **2002**, *295*, 1698; c) A. A. Kavitha, N. K. Singha, *ACS Appl. Mater. Interfaces* **2009**, *1*, 1427; d) P. Reutenauer, E. Buhler, P. J. Boul, S. J. Candau, J. M. Lehn, *Chem. - Eur. J.* **2009**, *15*, 1893; e) M. J. Barthel, T. Rudolph, A. Teichler, R. M. Paulus, J. Vitz, S. Hoeppener, M. D. Hager, F. H. Schacher, U. S. Schubert, *Adv. Funct. Mater.* **2013**, *23*, 4921; f) D. Arunbabu, S. M. Noh, J. H. Nam, J. K. Oh, *Macromol. Chem. Phys.* **2016**, *217*, 2191.

[12] a) C. e. Yuan, M. Z. Rong, M. Q. Zhang, Z. P. Zhang, Y. C. Yuan, *Chem. Mater.* **2011**, *23*, 5076; b) Z. P. Zhang, M. Z. Rong, M. Q. Zhang, C. E. Yuan, *Polym. Chem.* **2013**, *4*, 4648; c) K. Imato, A. Takahara, H. Otsuka, *Macromolecules* **2015**, *48*, 5632.

[13] a) H. Ying, J. Cheng, *J. Am. Chem. Soc.* **2014**, *136*, 16974; b) H. Ying, Y. Zhang, J. Cheng, *Nat. Commun.* **2014**, *5*, 3218.

[14] Y.-X. Lu, Z. Guan, *J. Am. Chem. Soc.* **2012**, *134*, 14226.

[15] a) S. H. Cho, S. R. White, P. V. Braun, *Chem. Mater.* **2012**, *24*, 4209; b) W. Schmolke, N. Perner, S. Seiffert, *Macromolecules* **2015**, *48*, 8781.

[16] a) J. J. Cash, T. Kubo, A. P. Bapat, B. S. Sumerlin, *Macromolecules* **2015**, *48*, 2098; b) O. R. Cromwell, J. Chung, Z. Guan, *J. Am. Chem. Soc.* **2015**, *137*, 6492.

[17] a) N. Kuhl, S. Bode, R. K. Bose, J. Vitz, A. Seifert, S. Hoeppener, S. J. Garcia, S. Spange, S. van der Zwaag, M. D. Hager, *Adv. Funct. Mater.* **2015**, *25*, 3295; b) P. Wang, G. Deng, L. Zhou, Z. Li, Y. Chen, *ACS Macro Lett.* **2017**, *6*, 881.

[18] a) S. Billiet, K. De Bruycker, F. Driessen, H. Goossens, V. Van Speybroeck, J. M. Winne, F. E. Du Prez, *Nat. Chem.* **2014**, *6*, 815; b) M. I. Lawton, K. R. Tillman, H. S. Mohammed, W. Kuang, D. A. Shipp, P. T. Mather, *ACS Macro Lett.* **2016**, *5*, 203; c) A. Susa, R. K. Bose, A. M. Grande, S. van der Zwaag, S. J. Garcia, *ACS Appl. Mater. Interfaces* **2016**, *8*, 34068; d) W.-X. Liu, C. Zhang, H. Zhang, N. Zhao, Z.-X. Yu, J. Xu, *J. Am. Chem. Soc.* **2017**, *139*, 8678; e) X. An, R. H. Aguirresarobe, L. Irusta, F. Ruiperez, J. M. Matxain, X. Pan, N. Aramburu, D. Mecerreyes, H. Sardon, J. Zhu, *Polym. Chem.* **2017**, *8*, 3641; f) Y. Cao, T. G. Morrissey, E. Acome, S. I. Allec, B. M. Wong, C. Keplinger, C. Wang, *Adv. Mater.* **2017**, *29*, 1605099; g) B. Zhang, P. Zhang, H. Zhang, C. Yan, Z. Zheng, B. Wu, Y. Yu, *Macromol. Rapid Commun.* **2017**, *38*, 1700110.

[19] a) J. Canadell, H. Goossens, B. Klumperman, *Macromolecules* **2011**, *44*, 2536; b) U. Lafont, H. Van Zeijl, S. van der Zwaag, *ACS Appl. Mater. Interfaces* **2012**, *4*, 6280; c) B. T. Michal, C. A. Jaye, E. J. Spencer, S. J. Rowan, *ACS Macro Lett.* **2013**, *2*, 694; d) Y. Amamoto, J. Kamada, H. Otsuka, A. Takahara, K. Matyjaszewski, *Angew. Chem., Int. Ed.* **2011**, *123*, 1698; e) Y. Amamoto, H. Otsuka, A. Takahara, K. Matyjaszewski, *Adv. Mater.* **2012**, *24*, 3975; f) Z. Q. Lei, H. P. Xiang, Y. J. Yuan, M. Z. Rong, M. Q. Zhang, *Chem. Mater.* **2014**, *26*, 2038.

[20] I. Azcune, I. Odriozola, *Eur. Polym. J.* **2016**, *84*, 147.

[21] L. Zhang, L. Chen, S. J. Rowan, *Macromol. Chem. Phys.* **2017**, *218*, 1600320.

[22] a) J. A. Yoon, J. Kamada, K. Koynov, J. Mohin, R. Nicolaÿ, Y. Zhang, A. C. Balazs, T. Kowalewski, K. Matyjaszewski, *Macromolecules* **2012**, *45*, 142; b) S. Y. An, S. M. Noh, J. H. Nam, J. K. Oh, *Macromol. Rapid Commun.* **2015**, *36*, 1255.

[23] H. Zeng, J. Huang, Y. Tian, L. Li, M. V. Tirrell, J. N. Israelachvili, *Macromolecules* **2016**, *49*, 5223.

[24] R. Wool, K. O'Connor, *J. Appl. Phys.* **1981**, *52*, 5953.

[25] A. M. Grande, J. C. Bijleveld, S. J. Garcia, S. van der Zwaag, *Polymer* **2016**, *96*, 26.

[26] M. S. Menyo, C. J. Hawker, J. H. Waite, *Soft Matter* **2013**, *9*, 10314.

[27] Y. J. Kwon, S. M. Hong, C. M. Koo, *J. Polym. Sci., Part B: Polym. Phys.* **2010**, *48*, 1265.

[28] K. Wissbrun, A. Griffin, *J. Polym. Sci., Polym. Phys. Ed.* **1982**, *20*, 1835.

[29] N. M. Patel, D. W. Dwight, J. L. Hedrick, D. C. Webster, J. E. McGrath, *Macromolecules* **1988**, *21*, 2689.

[30] D. P. Queiroz, A. B. do Rego, M. N. de Pinho, *J. Membr. Sci.* **2006**, *281*, 239.

[31] a) W. J. Yoon, S. Y. Hwang, J. M. Koo, Y. J. Lee, S. U. Lee, S. S. Im, *Macromolecules* **2013**, *46*, 7219; b) S.-A Park, J. Choi, S. Ju, J. Jegal, K. M. Lee, S. Y. Hwang, D. X. Oh, J. Park, *Polymer* **2017**, *116*, 153.

© 2017 WILEY-VCH Verlag GmbH & Co. KGaA, Weinheim